ACS Energy LETTERS

Cite This: ACS Energy Lett. 2018, 3, 1590−1596

LETTER

Design Principles for Directing Energy and Energetic Charge Flow in Multicomponent Plasmonic Nanostructures

Steven Chavez, Umar Aslam, and Suljo Linic*

Department of Chemical Engineering, University of Michigan—Ann Arbor, Ann Arbor, Michigan 48109, United States

Supporting Information

ABSTRACT: The decay of localized surface plasmons supported by plasmonic metal nanoparticles results in the formation of energetic charge carriers within the nanoparticles. Once formed, these charge carriers can transfer to chemically attached materials where they can perform a function. The efficient extraction and utilization of these charge carriers in various applications hinges on the ability to design plasmonic nanostructures with highly localized charge carrier generation at specific locations in the nanostructure. Herein, we shed light on the physical mechanisms governing the flow of energy in resonantly excited multimetallic plasmonic nanoparticles. We demonstrate that coating plasmonic nanostructures with nonplasmonic metals can result in the preferential dissipation of energy (i.e., formation of charge carriers) in the nonplasmonic metal and that the extent of this dissipation depends heavily on the electronic structure of the constituent metals. We use experimental and modeling studies of various core−shell nanostructures to develop a transparent physical framework of energy transfer in these systems and discuss how this framework can be used to engineer nanostructures that allow for high efficiencies of charge carrier extraction.

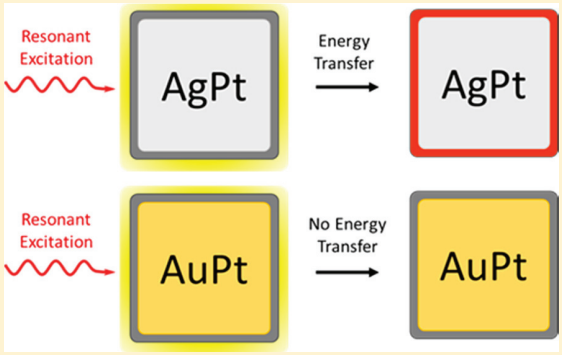

Plasmonic metal nanoparticles are promising platforms for manipulating the flow of electromagnetic energy at the nanometer length scale. Upon light illumination, incoming electromagnetic radiation interacts with the delocalized, free electrons of the metallic nanoparticles, resulting in excitation of the localized surface plasmon resonance (LSPR).[1−4] LSPR acts to confine the energy of incoming radiation in the form of amplified electromagnetic fields at the surface of the nanostructure.[5−7] The energy of these elevated fields is dissipated through either radiative scattering of photons or nonradiative excitation of energetic charge carriers (i.e., absorption) in the metal nanoparticle.

There is growing interest in developing a deeper understanding of the energy dissipation pathways in resonantly excited plasmonic nanoparticles with the ultimate aim of designing plasmonic nanostructures that offer a high degree of control over the LSPR decay process in terms of (1) the partitioning of energy between absorption and scattering and (2) the spatial distribution of the absorption process.[8−13] For example, manipulating the location of charge carrier excitation (photon absorption) in terms of surface versus bulk excitations is critical in a number of applications, including plasmonic photocatalysis,[14−21] plasmon-enhanced photovoltaics,[22−25] plasmonic heating,[26−28] and photothermal cancer therapy.[29−33] Ideally, these high-energy charge carriers would be generated close to the particle surface to minimize their energy loss within the nanoparticle before their extraction.

We recently described the design of a hybrid bimetallic plasmonic nanostructure that allows for a high degree of control over the LSPR decay mechanism in terms of absorption/scattering ratios and the location of the absorption process.[34] In these nanostructures, a very thin shell (1 nm) of a nonplasmonic metal (Pt) was coated onto a larger plasmonic nanoparticle core (75 nm Ag cube). We showed that the energy concentrated via LSPR excitation in the core−shell nanoparticle was preferentially dissipated through the absorption process in the thin Pt shell (i.e., within ∼1 nm of the bimetallic nanoparticle surface), increasing the extraction probability of the energetic charge carriers.

Herein, we focus on analyzing the physical framework describing the flow of energy in multimetallic plasmonic nanoparticles. We systematically investigate, through experimental and modeling approaches, the LSPR decay mechanisms in Ag−Pt and Au−Pt core−shell nanoparticles of

Received: May 22, 2018
Accepted: June 12, 2018
Published: June 12, 2018

DOI: 10.1021/acsenergylett.8b00841
ACS Energy Lett. 2018, 3, 1590−1596

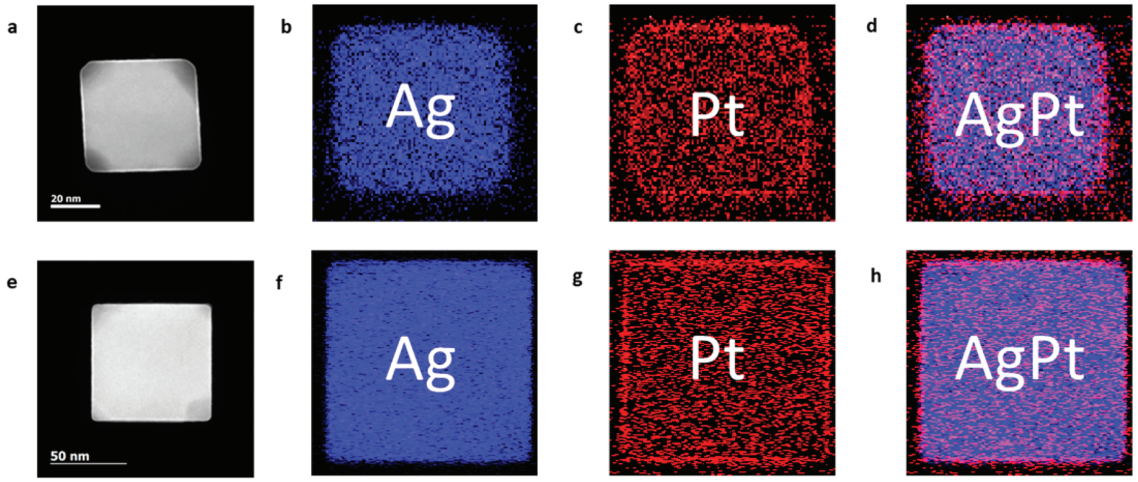

Figure 1. (a–d) Dark field STEM image of a representative small Ag–Pt nanocube. The average edge length of the nanocubes was ~41 ± 3 nm (a). EDS elemental maps of Ag (b) and Pt (c) and their overlay (d). (e–h) Dark field STEM image of a representative large Ag–Pt nanocube. The average edge length of the nanocubes was ~111 ± 1 nm (e). EDS elemental maps of Ag (f) and Pt (g) and their overlay (h).

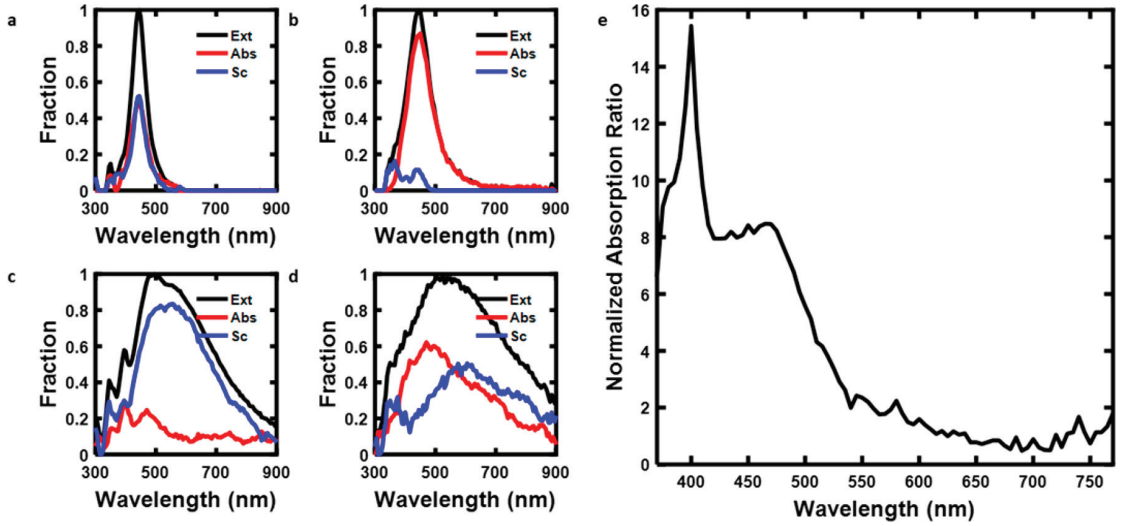

Figure 2. (a–d) Measured fractional extinction, absorption, and scattering of (a) small Ag cubes, (b) small Ag cubes coated with ~1.4 nm of Pt, (c) large Ag cubes, and (d) large Ag cubes coated with ~1.4 nm of Pt; (e) experimental volume-normalized absorption ratio in the Pt shells of the small to large particles.

different shapes and sizes. We demonstrate that the nanoparticle size significantly impacts the plasmon decay pathways, where particle sizes supporting higher electric field intensities at the nanoparticle surface direct more energy to Pt. We also show that the choice of plasmonic metal (Ag vs Au) strongly impacts the LSPR energy dissipation pathways. We demonstrate that, unlike for the Ag–Pt nanoparticles where the energy is dissipated through the Pt shell for all LSPR wavelengths, for the Au–Pt system a significant biasing of the particle absorption in Pt is only achieved at the LSPR wavelengths where the Au interband transitions are inaccessible. Collectively, these studies have allowed us to develop a transparent physical mechanism for the LSPR decay in multimetallic plasmonic nanostructures.

Ag nanocube seeds of varying sizes were synthesized using an established polyol method and characterized using high-angle annular dark field scanning transmission electron microscopy (HAADF-STEM).[35,36] The Ag nanocube seeds used in this study were ~40 nm in edge length (small particles) and ~110 nm in edge length (large particles). A thin layer of Pt was subsequently coated onto the surface of the Ag seeds using a recently reported method.[37] Dark field STEM images of the small and large Ag–Pt nanocubes are shown in Figure 1a,e. Energy-dispersive X-ray spectroscopy (EDS) elemental maps of the particles (Figure 1b–d;f–h) show complete coverage of the Ag nanocubes cores by the Pt shell. The average thickness of the Pt shell was determined to be 1.4 nm from the STEM images.

We measured the optical extinction, absorption, and scattering spectra of the small and large Ag and Ag–Pt nanocubes using transmission UV–vis spectroscopy and an optical integrating sphere. The data in Figure 2a show that for the small Ag nanocubes excited plasmons decay approximately equally through scattering and absorption, while the data in Figure 2c show that scattering is the dominant decay channel for larger Ag nanocubes. Comparing the extinction, absorption, and scattering of monometallic Ag nanocubes (Figure 2a,c) to that of Ag–Pt nanocubes (Figure 2b,d), it is clear that the

DOI: 10.1021/acsenergylett.8b00841
ACS Energy Lett. 2018, 3, 1590–1596

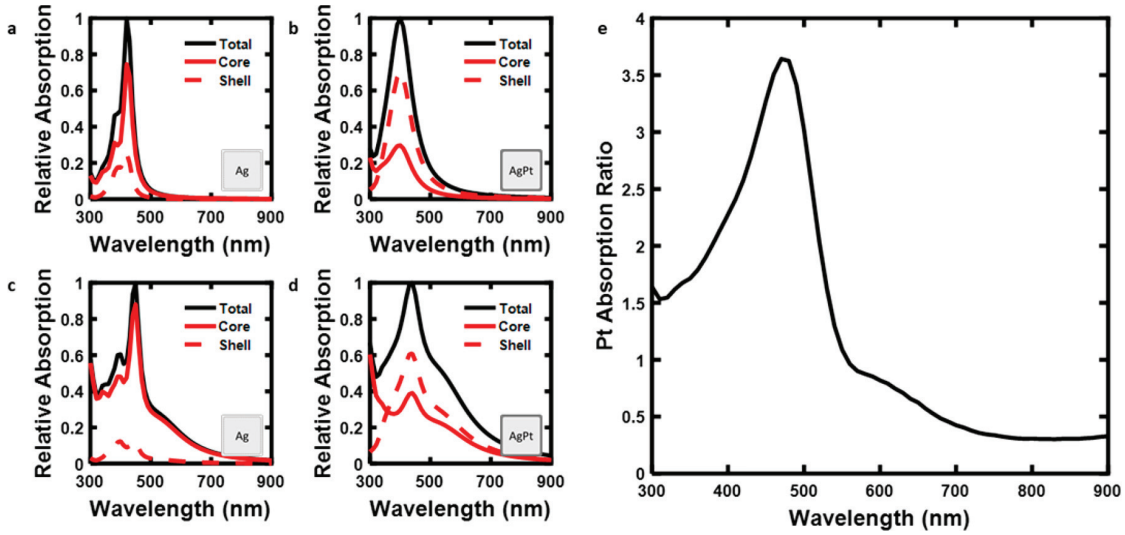

Figure 3. (a–d) Relative absorption fractions in the core vs the shell for (a) a 40 nm Ag cube with a 1.4 nm thick Ag shell: (b) a 40 nm Ag cube with a 1.4 nm thick Pt shell, (c) a 110 nm Ag cube with a 1.4 nm thick Ag shell, and (d) a 110 nm Ag cube with a 1.4 nm thick Pt shell. (e) Simulated volume-normalized absorption ratio in the Pt shell of the small to large particles.

absorption/scattering ratio increases significantly upon introduction of the thin Pt shell for both large and small particles. Together, the data from these optical measurements (Figure 2a–d) show that coating plasmonic Ag nanocubes with Pt alters the LSPR decay pathway, leading to significantly more absorption as opposed to scattering. We have shown previously that these changes in the absorption to scattering ratio are due to increased absorption in Pt compared to that in Ag, i.e., the plasmon energy is dissipated by absorption directly in the Pt shell.[34]

To investigate how the particle size affects the rate of energy dissipation through Pt, we estimated the experimental ratio of the volume-normalized absorption in the Pt shells for the two particle sizes. This is essentially a measure of the effectiveness of these bimetallic systems at dissipating electromagnetic energy through the Pt surface layers (i.e., the surface sites). We can crudely approximate this ratio using the following equation

$$\frac{\mathrm{Pt}_{\mathrm{Abs},40}}{\mathrm{Pt}_{\mathrm{Abs},110}} \approx \frac{A_{\mathrm{AgPt},40} - A_{\mathrm{Ag},40}}{V_{\mathrm{Pt},40}} \times \frac{V_{\mathrm{Pt},110}}{A_{\mathrm{AgPt},110} - A_{\mathrm{Ag},110}}$$

where $A_{\mathrm{Ag},40}$ and $A_{\mathrm{AgPt},40}$ are the experimental absorptions for the small Ag and Ag–Pt nanocubes, $A_{\mathrm{Ag},110}$ and $A_{\mathrm{AgPt},110}$ are the experimental absorptions for the large Ag and Ag–Pt nanocubes, and $V_{\mathrm{Pt},40}$ and $V_{\mathrm{Pt},110}$ are the volumes of the small and large Pt shells, respectively. The data in Figure 2e show that the Pt shell volume-normalized absorption ratio in the small versus large nanoparticles is significantly larger than 1 below ~640 nm and that it reaches close to 1 above this wavelength. This analysis suggests that below the wavelength of ~640 nm the smaller nanoparticles are much more effective in driving energy to the Pt shell.

To shed light on the experimentally observed difference in the rate of energy dissipation in the surface Pt atoms as a function of particle size, we performed finite element method (FEM) simulations on the systems of interest (simulation details are provided in the Supporting Information). The simulated optical characteristics (extinction, absorption, and scattering) of both small and large nanocubes (Figure S3a–d) are consistent with the experimental measurements (Figure 2a–d), showing that the nanoparticle absorption increases upon depositing Pt onto the surface of the Ag nanocube seeds. Because the FEM simulations allow us to compute the absorption in the different parts of the hybrid nanostructures, we also calculated the fractional absorption in the Pt shell vs the Ag core for each particle size and compared it to a pure Ag particle with a fictitious Ag "shell" of dimensions equal to the Pt dimensions in the Ag–Pt nanocubes. The fractional absorption for small (Figure 3a) and large Ag nanocubes (Figure 3c) shows that for pure monometallic Ag absorption occurs mainly in the particle core, i.e., a relatively small fraction of energy is absorbed by the few Ag layers close to the surface of the nanoparticles. It is clear that upon deposition of the Pt shell, the particle absorption is moved to the Pt shell for both small (Figure 3b) and large Ag–Pt nanocubes (Figure 3d). Furthermore, by normalizing the simulated wavelength-dependent absorption in the Pt shell by the shell volume for the different particle sizes (see the Supporting Information for calculation details), we computed the wavelength-dependent absorption ratio in the Pt shell for the two particle sizes. These data show that the absorption in the Pt shell is significantly greater in the small nanoparticles at short wavelengths (less than ~560 nm). These simulation results (Figure 3e) are qualitatively consistent with the experimental analysis (Figure 2e), showing that small particles dissipate significantly more optical energy per unit volume of Pt than the large particles.

One feature of plasmonic nanoparticles that is size-dependent at the conditions of LSPR is the intensity of the electric field at the surface of the nanoparticles.[8,38] To investigate the role of field enhancement on the LSPR decay mechanism, we used the FEM simulations to calculate the average electric field intensity $|E|^2$ at the particle surface as a function of wavelength for both large and small Ag nanocubes (Figure 4a). These data show that the field intensity, $|E|^2$, is significantly greater for small Ag nanocubes for the wavelengths at which the ratio of the volume-normalized absorption in the Pt shell of small to large particles (Figure 3e) is large. This direct mapping between the field intensity and the rate at which energy is deposited into the Pt surface layers suggests that the electric fields generated at the surface of plasmonic

DOI: 10.1021/acsenergylett.8b00841
ACS Energy Lett. 2018, 3, 1590–1596

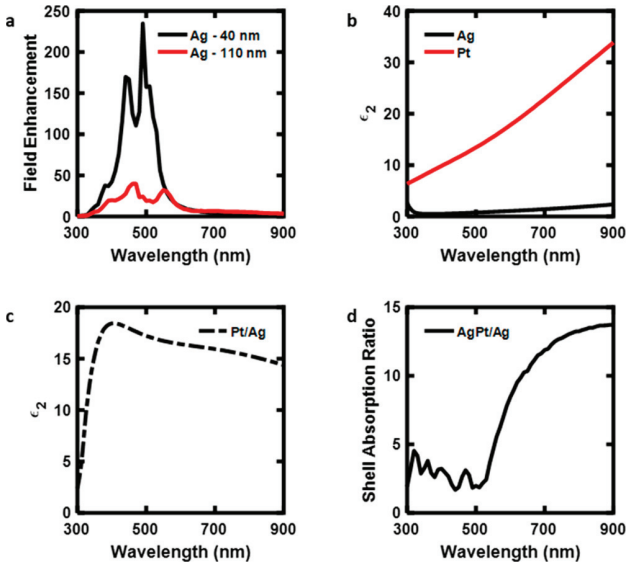

Figure 4. (a) Enhancement of the electric field intensity at the particle surface as a function of wavelength for small and large Ag nanocubes. (b) Imaginary part of the dielectric function for Ag and Pt as a function of wavelength; dielectric data taken from ref 18. (c) Wavelength-dependent ratio of the imaginary dielectric function of Pt with Ag. (d) Ratio of the calculated shell absorption for AgPt/Ag for the 40 nm particles.

particles at LSPR excitation frequencies play an important role in determining the rate at which the energy is transferred between the plasmonic nanostructure and an attached medium (in this case Pt).

Our data in Figure 2 also show that for a fixed particle size (either 40 or 110 nm) and shape the ratio of absorption to scattering increases for the Pt-coated particles compared to the pure Ag nanostructures. These observations cannot be entirely explained by the *E*-field intensity around the Ag plasmonic particles, and it is critical to examine additional factors, such as the electronic structure of Pt and Ag. Optical electronic excitations in metals can take place through either the excitation of s electrons below the Fermi level (E_f) to unoccupied s states above E_f (intraband transitions) or direct excitations of d electrons below E_f to unoccupied s states above E_f (interband transitions).[39] The probability of these optical excitations in a material is described by the imaginary part of the material's dielectric function (ε_2). The imaginary parts of the Pt and Ag dielectric functions are shown in Figure 4b.[40] It is clear that at the LSPR wavelengths Pt has a significantly larger ε_2 than Ag. This essentially means that under an identical set of conditions (e.g., identical optical field) the probability of a photon being absorbed by a Pt atom is significantly larger than the probability for photon absorption by a Ag atom. The main reason for this is that Ag is a d^{10} metal characterized by a populated d band lying far below E_f.[41] As a consequence, the excitation of d electrons to s states just above E_f (interband transitions) requires higher-energy photons than those provided at the LSPR wavelengths. Therefore, electronic excitations in Ag at these wavelengths are dominated by transitions between s states (intraband transitions), which require a third body to conserve momentum and are therefore characterized by low oscillator strengths (leading to low ε_2).[39] On the other hand, the d states for Pt are not completely full (Pt is a d^9 metal) and the d band intersects E_f.[42] This means that the d to s (interband) transitions in Pt can be activated at the LSPR wavelengths. In contrast to intraband transitions, interband transitions are direct, momentum-conserved excitations and are the main contributors to ε_2 of metals when available.[39,43] The availability of these transitions in Pt at visible wavelengths results in the large value of ε_2 for Pt compared to Ag.

In Figure 4c, we plotted the wavelength-dependent ratio of the Pt and Ag dielectric functions.[40] These data show that the value of ε_2 for Pt is between 15 and 18 times larger than the value for Ag in the visible range. To study the effect of this difference in ε_2 for Ag and Pt, we compared the shell absorption in a Ag−Pt core−shell nanocube to the absorption

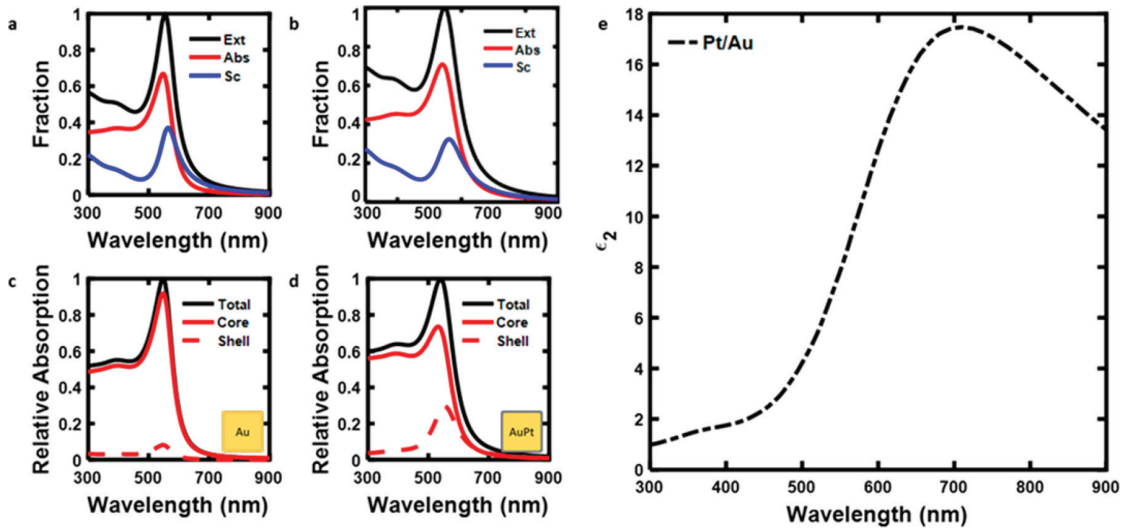

Figure 5. (a) Calculated extinction, absorption, and scattering fraction of a 75 nm edge length Au nanocube with a 1 nm Au shell. (b) Calculated extinction, absorption, and scattering fraction of a 75 nm edge length Au nanocube with a 1 nm Pt shell. (c,d) Relative absorption fractions in the core vs the shell for (c) a 75 nm Au cube with a 1 nm thick Au shell and (d) a 75 nm Au cube with a 1 nm thick Pt shell. (e) Wavelength-dependent ratio of the imaginary dielectric function of Pt with Au.

DOI: 10.1021/acsenergylett.8b00841
ACS Energy Lett. 2018, 3, 1590−1596

in the surface layers of a pure Ag nanocube of the same size. The data in Figure 4d show that the rate of absorption is always larger for a Pt shell compared to the Ag shell for an otherwise identical particle. This suggests that in these systems, where a plasmonic nanoparticle core is covered with a thin shell of a nonplasmonic metal, shell metals having a large value of ε_2 relative to the plasmonic metal open up a rapid LSPR dissipation pathway through the shell metal. We hypothesize that the availability of inherently fast direct electronic transitions (d to s) in these metals acts as a preferential decay pathway for the electric field energy stored at the nanoparticle surface under LSPR conditions. Physically, this manifests itself as highly efficient energy transfer from the plasmonic core to the nonplasmonic metal shell via direct absorption in the shell metal, which is characterized by a larger ε_2 relative to the plasmonic metal.

The analysis above paints a comprehensive picture of the photon absorption in multimetallic structures under LSPR conditions and informs us about how to design multifunctional materials that can guide the process of photon absorption to a particular spot in the material (i.e., the surface layers). It is clear that any such multicomponent material needs to be able to (i) concentrate the electric field to the surface, which can be accomplished by the plasmonic component at the LSPR wavelengths, and (ii) have another component at the surface (where the fields are high) characterized by a high imaginary part of the dielectric function relative to the plasmonic component at the LSPR wavelengths. To further probe this model, we used FEM modeling to analyze the optical characteristics of a 75 nm Au nanocube coated with 1 nm of Pt. This model system is analogous to the Ag−Pt core−shell system with Au substituted in place of Ag as the plasmonic metal core. The data in Figure 5a show the LSPR peak at ∼550 nm for these Au and Au−Pt nanocubes. The data in Figure 5a,b shows that, unlike in the Ag−Pt case, coating the Au nanocube with Pt does not significantly alter the plasmon decay pathway (i.e., absorption vs scattering). Additionally, the absorption fraction data in Figure 5c,d show that the presence of the thin Pt shell results in only marginal biasing of the plasmon decay pathway toward absorption in the Pt shell. This behavior is in contrast to that observed for the Ag−Pt nanoparticles (Figures 2 and 3) where the Pt shell provided a very effective pathway for plasmon decay via absorption. The key difference between Au and Ag is that Au has a higher ε_2 at these LSPR wavelengths, as shown in Figure 5e, where the ratio of ε_2 of Pt to Au as a function of wavelength is plotted. The data show that at ∼550 nm the ratio of ε_2 for Pt and Au is relatively low compared to the large ratios in ε_2 for Ag and Pt (Figure 4c). According to the model described above, this low ratio in the imaginary part of the dielectric function of Pt and Au indicates that a significant portion of the LSPR energy will be dissipated through absorption in Au, i.e., this Au particle geometry is not effective in driving energy into the surface Pt layers.

The model proposed above also suggests that moving the LSPR excitation frequency of the plasmonic Au core to longer wavelengths, where the ratio of Pt to Au ε_2 is high (Figure 5e), should preferentially direct more energy into the Pt shell. To probe this, we used FEM modeling to examine the behavior of a 20 nm × 80 nm Au nanorod coated with either 1 nm of Au or 1 nm of Pt. Plasmonic metal nanorods display two LSPR modes, a transverse mode with excitation frequencies at short wavelengths and a longitudinal mode with excitation frequencies at long wavelengths.[44,45] By varying the polarization of incident light in the FEM model, we can tune the LSPR frequency to regions where the ratio of Pt to Au ε_2 is low/high and can therefore study how the plasmon decay pathways are affected by the ratio of ε_2 of the constituent materials.

The data in Figure 6 show the normalized total absorption (solid lines) of the pure Au and Au−Pt nanorod as well as the

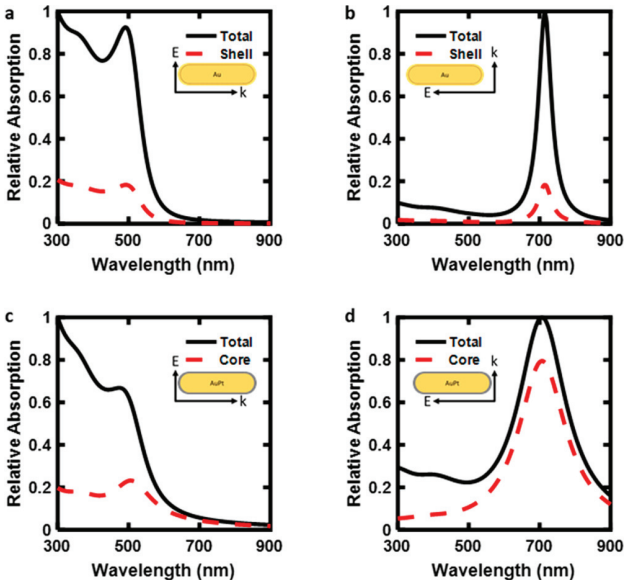

Figure 6. Relative absorption fractions of a Au and Au−Pt nanorod with a width of 20 nm coated with a 1 nm Au shell and 1 nm Pt shell, respectively. The nanorod length was 80 nm, corresponding to an aspect ratio (AR) of 2. The Au nanorod was illuminated with a plane wave polarized in the transverse direction (a) and in the longitudinal direction (b); the corresponding Au−Pt data for transverse and longitudinal polarizations are shown in (c) and (d). In all panels, the black solid lines represent the total particle absorption (normalized by the maximum absorption), and the red dotted lines represent the contribution of the total absorption that is attributed only to the shell. The insets depict the light propagation vector (k) and *E*-field polarization vector (E).

fractional absorption in the 1 nm Au shell of the pure Au nanorod and the 1 nm Pt shell of the Au−Pt nanorod (dotted lines) undergoing either longitudinal or transverse plasmon excitation. For the pure Au nanorod undergoing transverse plasmon excitation (Figure 6a), the shell absorption makes up a very low fraction of the total particle absorption. The same conclusions can be drawn for the pure Au nanorod undergoing longitudinal plasmon excitation (Figure 6b). The data show that when Pt is coated on the nanorod the flow of energy is strongly dependent on which plasmon mode is excited. The data in Figure 6c show that the transverse plasmon peak for the Au−Pt nanorod is located at ∼480 nm, where the ratio of ε_2 for Pt to Au is low. As a result, very little of the energy dissipation is moved to the Pt shell for the Au−Pt nanorod when this plasmon mode is excited. On the other hand, exciting the longitudinal plasmon mode shifts the LSPR wavelengths to regions where the Pt to Au ε_2 ratio is high. The data show that for the excitation of this plasmon mode a significant amount of the particle absorption comes from absorption directly in the Pt shell. Together, these data suggest that the LSPR energy can be dissipated through the

DOI: 10.1021/acsenergylett.8b00841
ACS Energy Lett. 2018, 3, 1590−1596

nonplasmonic metal shell when the value of ε_2 of the nonplasmonic metal is high relative to that of the plasmonic metal at the LSPR frequencies.

The results presented herein paint a clear picture of the physical mechanism governing energy transfer in multimetallic plasmonic nanostructures. By studying core−shell nanoparticles of varying size, shape, and composition, we demonstrated that the energy flow in multimetallic plasmonic nanostructures is dependent on two critical factors acting in concert: (i) the electric field intensity at the LSPR frequencies and (ii) the availability of direct transitions in the nonplasmonic metal relative to the plasmonic metal. To isolate the effect of the field intensity, we studied Ag−Pt and Ag nanocubes of varying sizes. We showed that nanoparticles displaying higher field intensities under LSPR conditions were more effective in dissipating energy through the nonplasmonic metal shell. Additionally, the extent of this energy transfer to the nonplasmonic shell depended on the ratio of ε_2 of the core and shell materials at the LSPR wavelength, where a higher shell to core ε_2 ratio resulted in more energy transfer to the shell. This framework allows for not only the design of hybrid nanostructures that localize charge carriers to desired parts of the nanostructure but also the generation and potential extraction of charge carriers that have entirely different energy distributions than those generated in plasmonic metals.

■ ASSOCIATED CONTENT

Supporting Information

The Supporting Information is available free of charge on the ACS Publications website at DOI: 10.1021/acsenergylett.8b00841.

Summary of nanoparticle synthesis, optical experiments, equations for calculations presented in the Letter, dielectric data, a description of the FEM simulations, and additional optical data (PDF)

■ AUTHOR INFORMATION

Corresponding Author

*E-mail: linic@umich.edu.

ORCID

Steven Chavez: 0000-0001-8469-625X

Umar Aslam: 0000-0001-8310-2958

Author Contributions

S.L., S.C., and U.A. conceived the project. S.C. carried out the syntheses, optical measurements, and all of the optical simulations. S.C. and U.A. performed the TEM characterization. All of the authors worked on the data analysis and conclusion development. All authors wrote the manuscript and Supporting Information.

Notes

The authors declare no competing financial interest.

■ ACKNOWLEDGMENTS

This work was primarily supported by the National Science Foundation (NSF) (CBET-1436056 and CBET- 1702471). The synthesis was developed with the support of the U.S. Department of Energy, Office of Basic Energy Science, Division of Chemical Sciences (FG-02-05ER15686). Secondary support for the development of analytical tools used to analyze the optical measurements was provided by the NSF (CBET-1437601). S.L. also acknowledges the partial support of the Technische Universität München − Institute for Advanced Study, funded by the German Excellence Initiative and the European Union Seventh Framework Programme under Grant Agreement No. 291763

■ REFERENCES

(1) Kelly, L.; Coronado, E.; Zhao, L.; Schatz, G. The Optical Properties of Metal Nanoparticles: The Influence of Size, Shape, and Dielectric Environment. *J. Phys. Chem. B* **2003**, *107*, 668−677.

(2) El-Sayed, M. Some Interesting Properties of Metals Confined in Time and Nanometer Space of Different Shapes. *Acc. Chem. Res.* **2001**, *34*, 257−264.

(3) Link, S.; El-Sayed, M. Spectral Properties and Relaxation Dynamics of Surface Plasmon Electronic Oscillations in Gold and Silver Nanodots and Nanorods. *J. Phys. Chem. B* **1999**, *103*, 8410−8426.

(4) Bohren, C. How Can a Particle Absorb More than the Light Incident on It? *Am. J. Phys.* **1983**, *51*, 323.

(5) Hao, E.; Schatz, G. Electromagnetic Fields around Silver Nanoparticles and Dimers. *J. Chem. Phys.* **2004**, *120*, 357−66.

(6) Linic, S.; Christopher, P.; Ingram, D. B. Plasmonic-Metal Nanostructures for Efficient Conversion of Solar to Chemical Energy. *Nat. Mater.* **2011**, *10*, 911−921.

(7) Schuller, J. A.; Barnard, E. S.; Cai, W.; Jun, Y. C.; White, J. S.; Brongersma, M. L. Plasmonics for Extreme Light Concentration and Manipulation. *Nat. Mater.* **2010**, *9*, 193−204.

(8) Li, K.; Hogan, N. J.; Kale, M. J.; Halas, N. J.; Nordlander, P.; Christopher, P. Balancing Near-Field Enhancement, Absorption, and Scattering for Effective Antenna−Reactor Plasmonic Photocatalysis. *Nano Lett.* **2017**, *17*, 3710−3717.

(9) Brown, A. M.; Sundararaman, R.; Narang, P.; Goddard, W. A.; Atwater, H. A. Nonradiative Plasmon Decay and Hot Carrier Dynamics: Effects of Phonons, Surfaces, and Geometry. *ACS Nano* **2016**, *10*, 957−966.

(10) Bernardi, M.; Mustafa, J.; Neaton, J. B.; Louie, S. G. Theory and Computation of Hot Carriers Generated by Surface Plasmon Polaritons in Noble Metals. *Nat. Commun.* **2015**, *6*, 7044.

(11) Simoncelli, S.; Li, Y.; Cortés, E.; Maier, S. A. Imaging Plasmon Hybridization of Fano Resonances via Hot-Electron-Mediated Absorption Mapping. *Nano Lett.* **2018**, DOI: 10.1021/acs.nanolett.8b00302.

(12) Joplin, A.; Hosseini Jebeli, S. A.; Sung, E.; Diemler, N.; Straney, P. J.; Yorulmaz, M.; Chang, W.; Millstone, J. E.; Link, S. Correlated Absorption and Scattering Spectroscopy of Individual Platinum-Decorated Gold Nanorods Reveals Strong Excitation Enhancement in the Nonplasmonic Metal. *ACS Nano* **2017**, *11*, 12346−12357.

(13) Swearer, D.; Zhao, H.; Zhou, L.; Zhang, C.; Robatjazi, H.; Martirez, J. M. P.; Krauter, C. M.; Yazdi, S.; McClain, M. J.; Ringe, E.; et al. Heterometallic Antenna−Reactor Complexes for Photocatalysis. *Proc. Natl. Acad. Sci. U. S. A.* **2016**, *113*, 8916−8920.

(14) Mubeen, S.; Lee, J.; Singh, N.; Kramer, S.; Stucky, G. D.; Moskovits, M. An Autonomous Photosynthetic Device in which all Charge Carriers Derive from Surface Plasmons. *Nat. Nanotechnol.* **2013**, *8*, 247−251.

(15) Christopher, P.; Xin, H.; Linic, S. Visible-Light-Enhanced Catalytic Oxidation Reactions on Plasmonic Silver Nanostructures. *Nat. Chem.* **2011**, *3*, 467.

(16) Christopher, P.; Xin, H.; Marimuthu, A.; Linic, S. Singular Characteristics and Unique Chemical Bond Activation Mechanisms of Photocatalytic Reactions on Plasmonic Nanostructures. *Nat. Mater.* **2012**, *11*, 1044−1050.

(17) Mukherjee, S.; Libisch, F.; Large, N.; Neumann, O.; Brown, L. V.; Cheng, J.; Lassiter, J. B.; Carter, E. A.; Nordlander, P.; Halas, N. J. Hot Electrons Do the Impossible: Plasmon-Induced Dissociation of H_2 on Au. *Nano Lett.* **2013**, *13*, 240−247.

(18) Linic, S.; Aslam, U.; Boerigter, C.; Morabito, M. Photochemical Transformations on Plasmonic Metal Nanoparticles. *Nat. Mater.* **2015**, *14*, 567−576.

DOI: 10.1021/acsenergylett.8b00841
ACS Energy Lett. 2018, 3, 1590−1596

(19) Holewinski, A.; Xin, H.; Nikolla, E.; Linic, S. Identifying Optimal Active Sites for Heterogenius Catalysis by Metal Alloys Based on Molecular Descriptors and Electronic Structure Engineering. *Curr. Opin. Chem. Eng.* **2013**, *2*, 312−319.
(20) Schweitzer, N.; Xin, H.; Nikolla, E.; Miller, J. T.; Linic, S. Establishing Relationships between Geometric Structure and Chemical Reactivity of Alloy Catalysis based on their Measured Electronic Structure. *Top. Catal.* **2010**, *53*, 348−356.
(21) Boerigter, C.; Campana, R.; Morabito, M.; Linic, S. Evidence and Implications of Direct Charge Excitation as the Dominant Mechanism in Plasmon-Mediated Photocatalysis. *Nat. Commun.* **2016**, *7*, 10545.
(22) Atwater, H. A.; Polman, A. Plasmonics for Improved Photovoltaic Devices. *Nat. Mater.* **2010**, *9*, 205−213.
(23) Mubeen, S.; Hernandez-Sosa, G.; Moses, D.; Lee, J.; Moskovits, M. Plasmonic Photosensitization of a Wide Band Gap Semiconductor: Converting Plasmons to Charge Carriers. *Nano Lett.* **2011**, *11*, 5548−5552.
(24) Catchpole, K. R.; Polman, A. Plasmonic Solar Cells. Opt. *Opt. Express* **2008**, *16*, 21793.
(25) Moskovits, M. The Case for Plasmon-Derived Hot Carrier Devices. *Nat. Nanotechnol.* **2015**, *10*, 6−8.
(26) Baffou, G.; Quidant, R. Thermo-Plasmonics: using Metallic Nanostructures as Nano-sources of Heat. *Laser Photon. Rev.* **2013**, *7*, 171−187.
(27) Carlson, M. T.; Khan, A.; Richardson, H. H. Local Temperature Determination of Optically Excited Nanoparticles and Nanodots. *Nano Lett.* **2011**, *11*, 1061−1069.
(28) Chen, X.; Chen, Y.; Yan, M.; Qiu, M. Nanosecond Photothermal Effects in Plasmonic Nanostructures. *ACS Nano* **2012**, *6*, 2550−2557.
(29) Hirsch, L. R.; Stafford, R. J.; Bankson, J. A.; Sershen, S. R.; Rivera, B.; Price, R. E.; Hazle, J. D.; Halas, N. J.; West, J. L. Nanoshell-Mediated Near-Infrared Thermal Therapy of Tumors under Magnetic Resonance Guidance. *Proc. Natl. Acad. Sci. U. S. A.* **2003**, *100*, 13549−13554.
(30) Huang, X.; El-Sayed, I.; Qian, W.; El-Sayed, M. A. Cancer Cell Imaging and Photothermal Therapy in the Near-Infrared Region by Using Gold Nanorods. *J. Am. Chem. Soc.* **2006**, *128*, 2115−2120.
(31) Ali, M. R. K.; Wu, Y.; Tang, Y.; Xiao, H.; Chen, K.; Han, T.; Fang, N.; Wu, R.; El-Sayed, M. A. Targeting Cancer Cell Integrins using Gold Nanorods in Photothermal Therapy Inhibits Migration through Affecting Cytoskeletal Proteins. *Proc. Natl. Acad. Sci. U. S. A.* **2017**, *114*, E5655−E5663.
(32) Carpin, L. B.; Bickford, L. R.; Agollah, G.; Yu, T.; Schiff, R.; Li, Y.; Drezek, R. A. Immunoconjugated Gold Nanoshell-Mediated Photothermal Ablation of Trastuzumab-resistant Breast Cancer Cells. *Breast Cancer Res. Treat.* **2011**, *125*, 27−34.
(33) El-Sayed, I. H.; Huang, X.; El-Sayed, M. A. Selective Laser Photo-Thermal Therapy of Epithelial Carcinoma using anti-EGFR Antibody Conjugated Gold Nanoparticles. *Cancer Lett.* **2006**, *239*, 129−135.
(34) Aslam, U.; Chavez, S.; Linic, S. Controlling Energy Flow in Multimetallic Nanostructures for Plasmonic Catalysis. *Nat. Nanotechnol.* **2017**, *12*, 1000−1005.
(35) Sun, Y.; Xia, Y. Shape-Controlled Synthesis of Gold and Silver Nanoparticles. *Science (Washington, DC, U. S.)* **2002**, *298*, 2176−2179.
(36) Christopher, P.; Linic, S. Shape- and Size-Specific Chemistry of Ag Nanostructures in Catalytic Ethylene Epoxidation. *ChemCatChem* **2010**, *2*, 78−83.
(37) Aslam, U.; Linic, S. Addressing Challenges and Scalability in the Synthesis of Thin Uniform Metal Shells on Large Metal Nanoparticle Cores: Case Study of Ag−Pt Core−Shell Nanocubes. *ACS Appl. Mater. Interfaces* **2017**, *9*, 43127−43132.
(38) Christopher, P.; Moskovits, M. Hot Charge Carrier Transmission from Plasmonic Nanostructures. *Annu. Rev. Phys. Chem.* **2017**, *68*, 379−398.
(39) Khurgin, J. B. How to Deal with the Loss in Plasmonics and Metamaterials. *Nat. Nanotechnol.* **2015**, *10*, 2−6.
(40) Rakić, A. D.; Djurišić, A. B.; Elazar, J. M.; Majewski, M. L. Optical Properties of Metallic Films for Vertical-Cavity Optoelectronic Devices. *Appl. Opt.* **1998**, *37*, 5271−5283.
(41) Kreibig, U.; Vollmer, M. Optical Properties of Metal Clusters. *Springer Ser. Mater. Sci.*; **1995**. DOI: 10.1007/978-3-662-09109-8
(42) Hammer, B.; Nørskov, J. K. Theoretical Surface Science and Catalysis—Calculations and Concepts. *Adv. Catal.* **2000**, *45*, 71−129.
(43) Boerigter, C.; Aslam, U.; Linic, S. Mechanism of Charge Transfer from Plasmonic Nanostructures to Chemically Attached Materials. *ACS Nano* **2016**, *10*, 6108−6115.
(44) Eustis, S.; El-Sayed, M. A. Why Gold Nanoparticles are More Precious than Pretty Gold: Noble Metal Surface Plasmon Resonance and its Enhancement of the Radiative and Nonradiative Properties of Nanocrystals of Different Shapes. *Chem. Soc. Rev.* **2006**, *35*, 209−215.
(45) Jana, N.; Gearheart, L.; Murphy, C. J. Wet Chemical Synthesis of High Aspect Ratio Cylindrical Gold Nanorods. *J. Phys. Chem. B* **2001**, *105*, 4065−4067.

DOI: 10.1021/acsenergylett.8b00841
ACS Energy Lett. 2018, 3, 1590−1596